#### Log Number: 180

# IN-SUBCHANNEL TWO-DIMENSIONAL FLOW STRUCTURE INDUCED BY BUBBLE-LIQUID INTERFACIAL FORCES

T. Ikeno<sup>1</sup>, T. Sasakawa<sup>1</sup> and I. Kataoka<sup>2</sup>

<sup>1</sup> Nuclear Fuel Industries, Ltd., Kumatori, Osaka, Japan

<sup>2</sup> Osaka University, Suita, Osaka, Japan

t-ikeno@nfi.co.jp, sasakawa@nfi.co.jp, kataoka@mech.eng.osaka-u.ac.jp

#### **Abstract**

Flow structure induced by bubble-liquid interfacial forces was investigated by using a two-dimensional CMFD technique. The mass, momentum, turbulence energy and bubble diffusion equations were used as the fundamental equations. The basis for these equations was the two-fluid model: the equation of liquid phase was picked up from the equation system theoretically derived for the gas-liquid two-fluid turbulent flow. Existing interfacial force models were newly introduced into the cross-sectional momentum equations. Asymmetry of non-circular channel like sub-channel caused cross-sectional flow patterns which varied with balance among the interfacial forces. The flow structure characterized void fraction distribution in sub-channel.

## 1. Introduction

Phase distribution in gas-liquid two-phase turbulent flow is important factor for designing nuclear fuel assemblies. The subchannel is a unit flow channel surrounded by fuel rods or thimble tube, and the geometrical effect in subchannel characterizes the liquid velocity and phase distribution in the fuel assemblies. This paper addresses the effect of subchannel geometry on flow structure in two-phase turbulent flow.

Famous effect of subchannel geometry is the secondary flow, and it is a cross sectional average of 3-dimesional coherent structure of turbulence in subchannel [1]. In the gas-liquid two-phase turbulent flow, the gas phase complicatedly interacts with liquid phase [2]. Investigating the effect of secondary flow in two-phase turbulence was therefore useful for clarifying the effect of subchannel geometry [3]. The result showed that two-phase turbulence structure in subchannel was appeared as cross sectional flow, and then it affects the void fraction distribution [3].

Interfacial force is a key concept to explain the inter phase behaviors. Interfacial forces acting in a steady state flow were categorized into turbulent dispersion, wall and lift forces. The interfacial forces, in particular the lift force, has been used to explain the void fraction profile transition between the wall peak and core peak in circular tube geometry [4-5].

In this study, the effect of subchannel geometry on phase distribution is investigated focusing on cross sectional flow structure caused by the interfacial forces. To observe the phase distribution and flow structure, a computational multi fluid dynamics (CMFD) code developed for bubbly turbulent flow in subchannel [6] is used. The interfacial forces are introduced into the cross-sectional momentum equations. To investigate the geometrical effect, computational results for annular tube and subchannels are compared.

In the following sections, nomenclature, fundamental equations, computational method and computational results are explained. The concluding remarks are given in the final section.

#### 2. Nomenclature

 $C_D$ : Drag coefficient

 $d_{\scriptscriptstyle B}$ : Bubble diameter

 $D_{H}$ : Hydraulic equivalent diameter

 $D_{in}$ : Inner diameter of annular tube

 $D_{out}$ : Outer diameter of annular tube

 $d_{\scriptscriptstyle R}$ : Bubble diameter

g: Gravity acceleration

k: Turbulence energy

 $K_1, K_2$ : Constants

 $l_{TP}$ : Mixing length of two-phase flow

 $l_{SP}$ : Mixing length of single-phase flow

L: Heated length

 $N_{\varepsilon}$ : Grid number in the  $\xi$  direction

 $N_n$ : Grid number in the  $\eta$  direction

P: Rod to rod pitch

p: Pressure

u: Velocity in the x-coordinate

 $u_{\tau}$ : Average friction velocity

*U* : Contra-variant velocity on the  $\xi$  -  $\eta$  plane

 $U_T$ : Terminal velocity of single bubble in infinite media

v: Velocity in the y -coordinate

V: Contra-variant velocity on the  $\xi$  -  $\eta$  plane

w: Velocity in the z-coordinate

(Greek symbols)

 $\alpha$ : Void fraction

 $\beta_1, \beta_2, \gamma_1$ : Constants

 $\rho$ : Density

 $\sigma$ : Surface tension

 $\nu$ : Kinematic viscosity

(Subscripts)

G: Gas

L: Liquid

# 3. Computational Methods

# 3.1 Coordinate System

The computational domain is shown in Fig.1. It covers an octa-symmetric area of annular tube and sub-channel ( $0 \le \theta \le 45$  degrees) on the two-dimensional plane. The subchannel is open geometry unlike the annular tube, and it needs validation of the domain size for computation. Figure 1 shows the domain large enough for the steady Reynolds averaged Navier-Stokes (RANS) simulation because its equation mathematically keeps spatial symmetry. On the other hand, the unsteady simulation of Navier-Stokes equation like the large eddy simulation (LES), where the temporal derivative term can cause the symmetry to break, requires larger computational domain up to that covering 2 sub-channels [1]. This study employs the turbulence model based on the steady RANS formulation as described in Section 3.3.

As shown in Fig1(a), the computational domain for the annular tube is bounded by two wall surfaces (r=D/2, P/2). As shown in Fig.1(b), the computational domain for the subchannel is bounded by a wall surface (r=D/2) and three symmetrical axes, and the symmetrical boundaries are represented by  $\{r,\theta \mid \theta=0^\circ\}$ ,  $\{r,\theta \mid \theta=45^\circ\}$  and  $\{r,\theta \mid r\cos\theta=P/2\}$ . As shown in Fig.2, the coordinate systems x-y and  $\xi$ - $\eta$  are applied to the physical and calculation spaces, respectively. The Jacobian and the contra-variant velocities are as follows.

$$J = x_{\varepsilon} y_{\eta} - x_{\eta} y_{\varepsilon}, \tag{1}$$

$$U = \xi_x u_L + \xi_y v_L, \tag{2}$$

$$V = \eta_x u_L + \eta_y v_L. \tag{3}$$

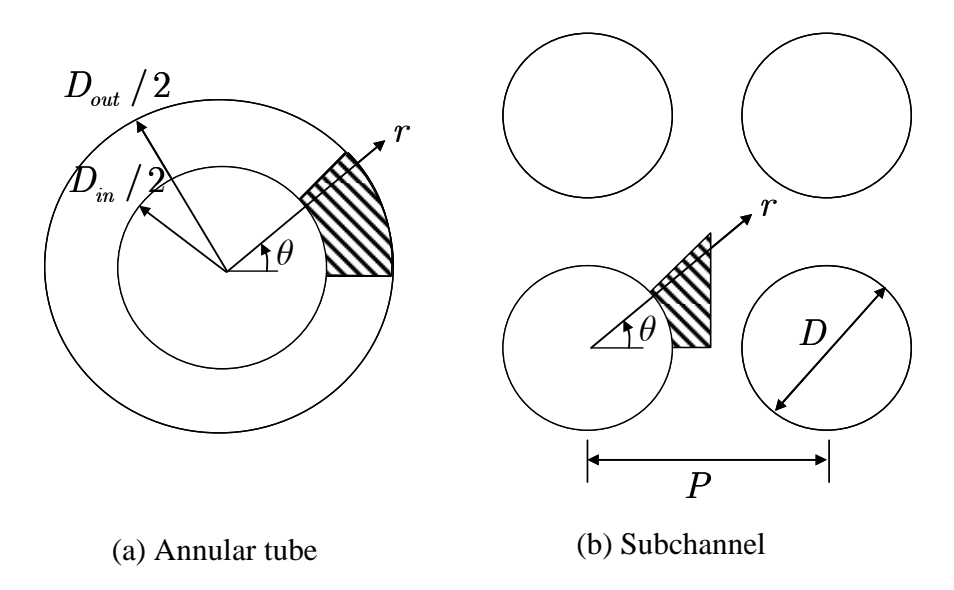
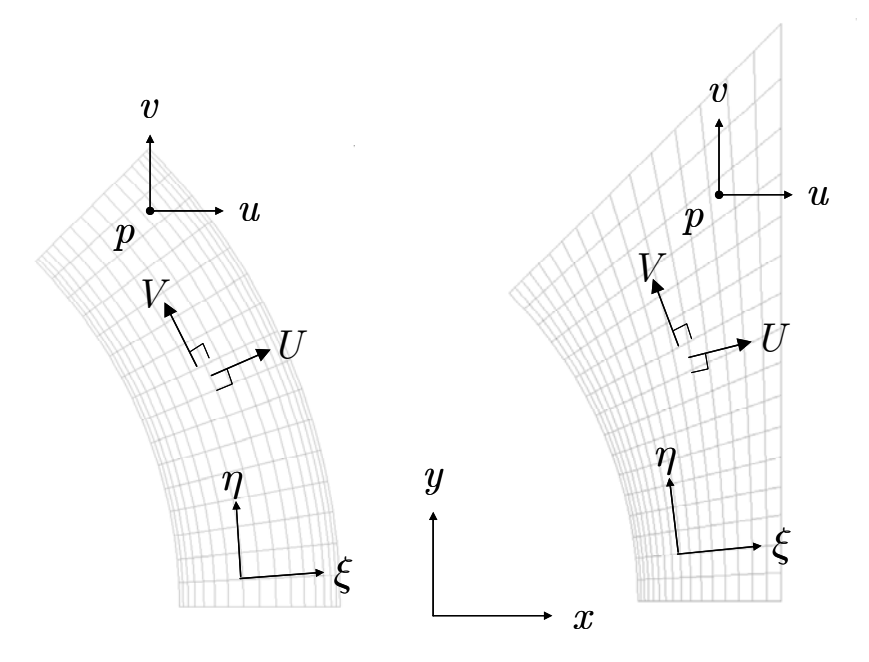


Fig.1 Computational domain in sub-channel.



(a) Annular tube (b) Subchannel Fig.2 Cartesian and generalized coordinates for physical and calculation spaces

## 3.2 Conservation Laws

The interfacial forces are introduced into the momentum equation. The momentum equations for cross-sectional velocities are

$$\frac{\partial}{\partial \xi} \left( J(1-\alpha) \rho_L U u_L \right) + \frac{\partial}{\partial \eta} \left( J(1-\alpha) \rho_L V u_L \right) \\
= \frac{\partial}{\partial \xi} \left\{ (1-\alpha) \nu_L \rho_L J \left( q_{11} \frac{\partial u_L}{\partial \xi} + q_{12} \frac{\partial u_L}{\partial \eta} \right) \right\} + \frac{\partial}{\partial \eta} \left\{ (1-\alpha) \nu_L \rho_L J \left( q_{21} \frac{\partial u_L}{\partial \xi} + q_{22} \frac{\partial u_L}{\partial \eta} \right) \right\} \\
- J(1-\alpha) \left( \xi_x \frac{\partial p}{\partial \xi} + \eta_x \frac{\partial p}{\partial \eta} \right) - J M_x^i$$
(4)

and

$$\begin{split} &\frac{\partial}{\partial \xi} \left( J \left( 1 - \alpha \right) \rho_L U v_L \right) + \frac{\partial}{\partial \eta} \left( J \left( 1 - \alpha \right) \rho_L V v_L \right) \\ &= \frac{\partial}{\partial \xi} \left\{ \left( 1 - \alpha \right) \nu_L \rho_L J \left( q_{11} \frac{\partial v_L}{\partial \xi} + q_{12} \frac{\partial v_L}{\partial \eta} \right) \right\} + \frac{\partial}{\partial \eta} \left\{ \left( 1 - \alpha \right) \nu_L \rho_L J \left( q_{21} \frac{\partial v_L}{\partial \xi} + q_{22} \frac{\partial v_L}{\partial \eta} \right) \right\} \\ &- J \left( 1 - \alpha \right) \left[ \xi_y \frac{\partial p}{\partial \xi} + \eta_y \frac{\partial p}{\partial \eta} \right] - J M_y^i \end{split} \tag{5}$$

Here,

$$q_{11} = \xi_x^2 + \xi_y^2, \tag{6}$$

$$q_{12} = \xi_x \eta_x + \xi_y \eta_y = q_{21}, \tag{7}$$

$$q_{22} = \eta_x^2 + \eta_y^2, \tag{8}$$

and  $M_x^i$  and  $M_y^i$  are the interfacial forces.

The momentum equation for axial velocity is

$$\frac{\partial}{\partial \xi} \left( J (1 - \alpha) \rho_L U w_L \right) + \frac{\partial}{\partial \eta} \left( J (1 - \alpha) \rho_L V w_L \right) 
= \frac{\partial}{\partial \xi} \left\{ J (1 - \alpha) \left( \nu_L + \beta_1 \sqrt{k} l_{TP} \right) \rho_L \left( q_{11} \frac{\partial w_L}{\partial \xi} + q_{12} \frac{\partial w_L}{\partial \eta} \right) \right\} 
+ \frac{\partial}{\partial \eta} \left\{ J (1 - \alpha) \left( \nu_L + \beta_1 \sqrt{k} l_{TP} \right) \rho_L \left( q_{21} \frac{\partial w_L}{\partial \xi} + q_{22} \frac{\partial w_L}{\partial \eta} \right) \right\} 
+ J \cdot \left\{ \frac{4\rho_L u_\tau^2}{D_H} - g \left\{ \tilde{\rho} - \overline{\rho} \right\} \right\}$$
(9)

where

$$\tilde{\rho} = \alpha \rho_G + (1 - \alpha) \rho_L, 
\bar{\rho} = \bar{\alpha} \rho_G + (1 - \bar{\alpha}) \rho_L.$$
(10)

The variable  $\sqrt{k}l_{TP}$  is a multiplication of turbulent velocity and mixing length, and it represents the effective turbulence viscosity.

The diffusion equation of bubble[7] [8] is

$$\frac{\partial}{\partial \xi} (J \rho_G U \alpha) + \frac{\partial}{\partial \eta} (J \rho_G V \alpha) 
= \frac{\partial}{\partial \xi} \left\{ \rho_G D_B J \left( q_{11} \frac{\partial \alpha}{\partial \xi} + q_{12} \frac{\partial \alpha}{\partial \eta} \right) \right\} + \frac{\partial}{\partial \eta} \left\{ \rho_G D_B J \left( q_{21} \frac{\partial \alpha}{\partial \xi} + q_{22} \frac{\partial \alpha}{\partial \eta} \right) \right\},$$

$$-J \alpha \rho_G w_G / L$$
(12)

where

$$D_B = \frac{1}{3} d_B w_L' = d_B \sqrt{\frac{2}{27} k_L} \ . \tag{13}$$

The last term in the right-hand side of Eq.(12) represents an axial gradient of mass velocity of the gas phase. It is introduced to simulates a cross-sectional slice of the two-phase flow developing along the heated rod [6]. Here,  $w_G$  in the third term of Eq.(12) is approximated by  $w_L + U_T$ . Namely, the terminal velocity for a single bubble is used as a gas-liquid relative velocity. The terminal velocity given by Ishii [9] is

$$U_{T} = \sqrt{2} \left\{ \sigma g (\rho_{L} - \rho_{G}) / \rho_{L}^{2} \right\}^{1/4}. \tag{14}$$

# 3.3 Turbulence Model

The turbulence energy and momentum equations are written for liquid phase. The turbulence energy equation is based on a one-equation mixing length model [10]. Although the mixing length model is hardly used in the recent single-phase turbulence simulation, its simple

formulation has been adaptable for representing two-phase modification by using experimental data [10][11].

The equation for turbulence energy of liquid phase is written as follows.

$$\frac{\partial}{\partial \xi} \left( J(1-\alpha) \rho_L U k_L \right) + \frac{\partial}{\partial \eta} \left( J(1-\alpha) \rho_L V k_L \right) \\
= \frac{\partial}{\partial \xi} \left\{ J(1-\alpha) \rho_L \left( \frac{\nu_L}{2} + \beta_2 \sqrt{k} l_{TP} \right) \left( q_{11} \frac{\partial k_L}{\partial \xi} + q_{12} \frac{\partial k_L}{\partial \eta} \right) \right\} \\
+ \frac{\partial}{\partial \eta} \left\{ J(1-\alpha) \rho_L \left( \frac{\nu_L}{2} + \beta_2 \sqrt{k} l_{TP} \right) \left( q_{21} \frac{\partial k_L}{\partial \xi} + q_{22} \frac{\partial k_L}{\partial \eta} \right) \right\} \\
+ J\beta_1 \sqrt{k_L} l_{TP} (1-\alpha) \left\{ \left( \frac{\delta w_L}{\delta \xi} + \eta_x \frac{\partial w_L}{\partial \eta} \right)^2 + \left( \xi_y \frac{\partial w_L}{\partial \xi} + \eta_y \frac{\partial w_L}{\partial \eta} \right)^2 \right\} - J\rho_L \varepsilon_L$$
(15)

where

$$\varepsilon_L = \{ \gamma_1 (1 - \alpha) / l_{TP} + K_2 \alpha / d_B \} k^{3/2} + 3K_1 \alpha C_D U_T^3 / (4d_B).$$
 (16)

The mixing length of two-phase flow is given by [11]

$$l_{TP} = l_{SP} + \frac{1}{3} d_B \alpha \,,$$
 (17)

where  $l_{SP}=0.4R$ ; R is the distance from the rod wall. The constants are  $K_1=2.0$ ,  $K_2=2.0$ ,  $\beta_1=0.4$ ,  $\beta_2=0.15$ ,  $\gamma_1=0.06$ . Here, the constants  $K_1$  and  $K_2$  in Eq.(16) both relate to the bubble induced turbulence term, which were derived from the interfacial energy transfer terms [12]. The term  $3K_1\alpha C_DU_T^{-3}/(4d_B)$  represents the turbulence generation due to bubble motion against the drag force. This term is quite important for determining the turbulence structure, particularly in the flow far from the wall [11]. The term  $K_2\alpha/d_Bk^{3/2}$  represents the turbulence absorption, where the interfacial area concentration was assumed to be proportional to void fraction and liquid fluctuation [10].

## 3.4 Interfacial forces

Turbulent diffusion and lift forces are picked up for the interfacial force in Eq.(4)(5). The turbulent diffusion force is represented by [4]:

$$M^{TD} = -C_{TD}\rho_c k\alpha_k \frac{\partial \alpha}{\partial r} + C_{TD,k}\rho_c (1 - \alpha)\alpha_k \frac{\partial k}{\partial r} \quad (k = 1, 2) \qquad , \tag{18}$$

$$M^{TD} = -C_{TD}\rho_c k\alpha_k \frac{\partial \alpha}{\partial r} \quad (k = 3, 4) \tag{19}$$

where  $C_{\rm TD}=5C_{\rm L}\,(k=1,2)$ ,  $C_{\rm TD}=0.6C_{\rm L}\,(k=3,4)$ . The lift force is represented by:

$$M^{L} = -C_{L}\rho_{c}\alpha_{k}u_{ref}\frac{\partial u_{l}}{\partial r},$$

where  $C_L=0.03 \, (k=1,2)$ ,  $C_L=-0.001 (k=3)$ ,  $C_L=-0.2 \, (k=4)$ . The bubble size group are represented by k=1,2,3,4 for the bubble diameter of  $0 < d_B < 4.8 mm$ ,  $4.8 mm < d_B < 5.8 mm$ ,  $5.8 mm < d_B < 7 mm$ ,  $7 mm < d_B$ , respectively [4].

The derivation by r in Eqs.(14) and (15) represents the gradient, and these equations are rewritten as:

$$\begin{split} M_x^i &= -C_{TD}\rho_c k\alpha_k \left(\xi_x \frac{\partial \alpha}{\partial \xi} + \eta_x \frac{\partial \alpha}{\partial \eta}\right) + C_{TD,k}\rho_c \left(1 - \alpha\right)\alpha_k \left(\xi_x \frac{\partial k}{\partial \xi} + \eta_x \frac{\partial k}{\partial \eta}\right) \\ &- C_L \rho_c \alpha_k u_{ref} \left(\xi_x \frac{\partial u_l}{\partial \xi} + \eta_x \frac{\partial u_l}{\partial \eta}\right) \\ M_y^i &= -C_{TD}\rho_c k\alpha_k \left(\xi_y \frac{\partial \alpha}{\partial \xi} + \eta_y \frac{\partial \alpha}{\partial \eta}\right) + C_{TD,k}\rho_c \left(1 - \alpha\right)\alpha_k \left(\xi_y \frac{\partial k}{\partial \xi} + \eta_y \frac{\partial k}{\partial \eta}\right) \\ &- C_L \rho_c \alpha_k u_{ref} \left(\xi_x \frac{\partial u_l}{\partial \xi} + \eta_x \frac{\partial u_l}{\partial \eta}\right) \end{split}.$$

#### 3.5 Finite Volume Procedure

As shown in Fig.2, the collocated grid system on the generalized coordinate  $\,\xi$ - $\eta$  is used. In each computational cell, the pressure and the Cartesian velocity is located at the center, and the contra-variant velocity is located on the side. In Fig.2(a), which shows annular tube, the wall boundaries  $\,\{r,\theta\mid r=D_{in}\,/\,2,D_{out}\,/\,2\}\,$  are represented by  $\,\xi=0,N_{\xi}\,$  and, and the symmetrical boundary  $\,\{r,\theta\mid\theta=0,\pi\,/\,4\}\,$  is represented by  $\,\eta=0,N_{\eta}\,$ . In Fig.2(b), which shows subchannel, the wall boundary  $\,\{r,\theta\mid r=D/2\}\,$  is represented by  $\,\xi=0\,$ . The symmetrical boundaries  $\,\{r,\theta\mid\theta=45^\circ\},\{r,\theta\mid\theta=0\}\,$  and  $\,\{r,\theta\mid r\cos\theta=P/2\}\,$  are then represented by  $\,\eta=0,N_{\eta}\,$  and  $\,\xi=N_{\xi}\,$ , respectively. The grid spacing for both  $\,\xi$ - $\,\eta\,$  directions is set at the unity to simplify the discrete equations.

To maintain the mass conservation for  $u_L$  and  $v_L$ , a pressure correction based on the SIMPLE (Semi-Implicit method for Pressure-Linked Equations[13]) is performed. Using the finite volume method, the equation for the pressure corrector and Eqs. (4), (5), (9), (12) and (15) are discretized into algebraic equations. An iterative under-relaxation method for tri-diagonal matrix is applied to each of those algebraic equations. Outer iteration through overall the equation system is continued until the change in the solution converges within 0.01 percent. The grid number used in the computation is  $N_\xi \times N_\eta = 16 \times 16$  for annular tube and  $32 \times 32$  for subchannel.

The orthogonal nature of the computational mesh is important to exactly simulate the boundary condition. The shape of sub-channel causes a distortion of the computational mesh, and orthogonal nature sometimes broken. In particular, it is difficult to keep the orthogonal nature on

the symmetrical boundaries  $\{r,\theta \mid r\cos\theta = P/2\}$  and  $\{r,\theta \mid \theta = 45^\circ\}$  in Fig.2(b). If the priority is given to the orthogonal nature, the size of adjacent cells becomes so different that it brings another numerical inaccuracy. To avoid this, an iterative method to keep the symmetry on the non-orthogonal boundary [3] is used.

# 3.6 Boundary Conditions

To simulate the flow at the high Reynolds number condition, the wall boundary for axial velocity and kinetic energy is represented by the log-law, which gives the value at the first grid. Predicting the wall void fraction using a boiling model [14] is possible, however this study places it as a future work. The cross-sectional flow is slow enough, and the no-slip wall condition is applied on the rod surface. For all the parameters, the gradient free condition to represent the symmetry is given at other boundaries.

# 4. Computational Results

In order to investigate the effect of geometry, computations are performed for annular tube and subchannel. The mass flux is  $3000~{\rm kg/m^2s}$  and the Reynolds number, based on mean velocity and hydraulic equivalent diameter, is 38000. Thermal property at  $25~{\rm degrees}$  Celsius and  $1~{\rm kgf/cm^2}$  are used:  $\rho_L=959.02~{\rm kg/m^3},~\rho_G=0.57966~{\rm kg/m^3},~\sigma=71.972\times10^{-3}~{\rm N/m},$   $\nu=0.92812\times10^{-6}~{\rm m^2/s},~h_{fg}=2258.9~{\rm kJ/kg}.$ 

#### 4.1 Annular tube

The computational results for annular tube are shown in Fig.3. The cross sectional vector shows unphysical flow structure with a scale smaller than  $10^{-2}$ , which is considered numerical error. There are thus no effective cross sectional flow in the annular tube geometry. As a result of this, the distribution of liquid velocity and void fraction is independent of bubble size and keeps similarity with geometry. The result is consistent with that of existing experiment, where the void fraction distribution in a heated annular tube showed independence on the interfacial forces [15]. In this symmetric geometry, the interfacial forces does not cause any cross sectional flows and only the heat flux dominate the phase distribution.

#### 4.2 Subchannel

The computational results for subchannel are shown in Fig.4. The cross sectional vectors show flow patterns depending on bubble sizes. The results for large and medium bubble size show flow structure similar to the secondary flow of the Prandtle's second kind [3]. The flow turns from the wall to subchannel center and then to the rod gap. This flow causes the flat void fraction distribution in subchannel even with heated rod. The doublet flow pattern for the medium size bubble is caused by the lift force weaker than that of large bubble size. The result for small bubble size show a flow turning in the direction opposite to that of the secondary flow of the Prandtle's second kind [3]. This causes a modified wall peak void fraction distribution characteristic of subchannel gemometry. The flow pattern is not similar with its geometry.

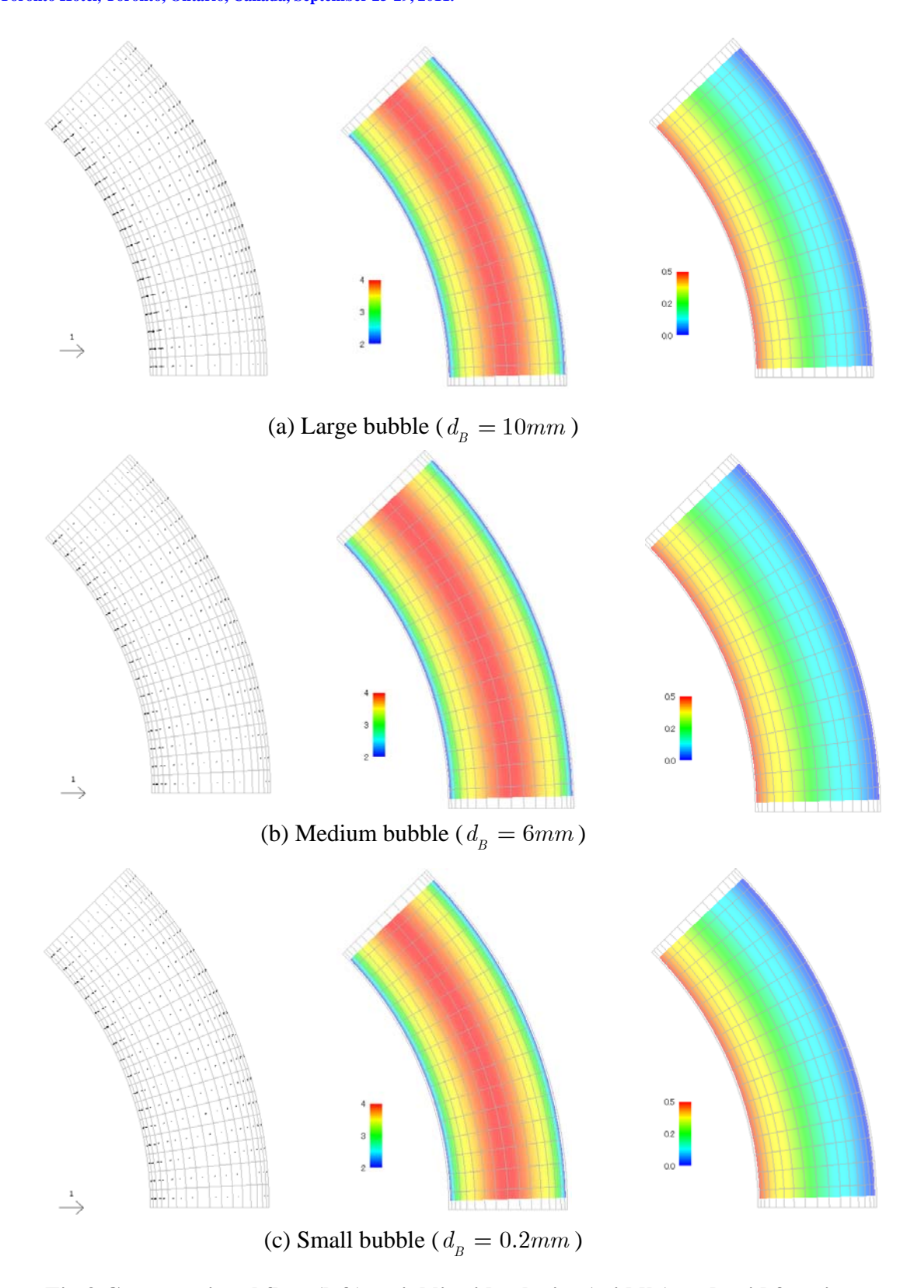


Fig.3 Cross sectional flow (left), axial liquid velocity (middle) and void fraction (right) in annular tube

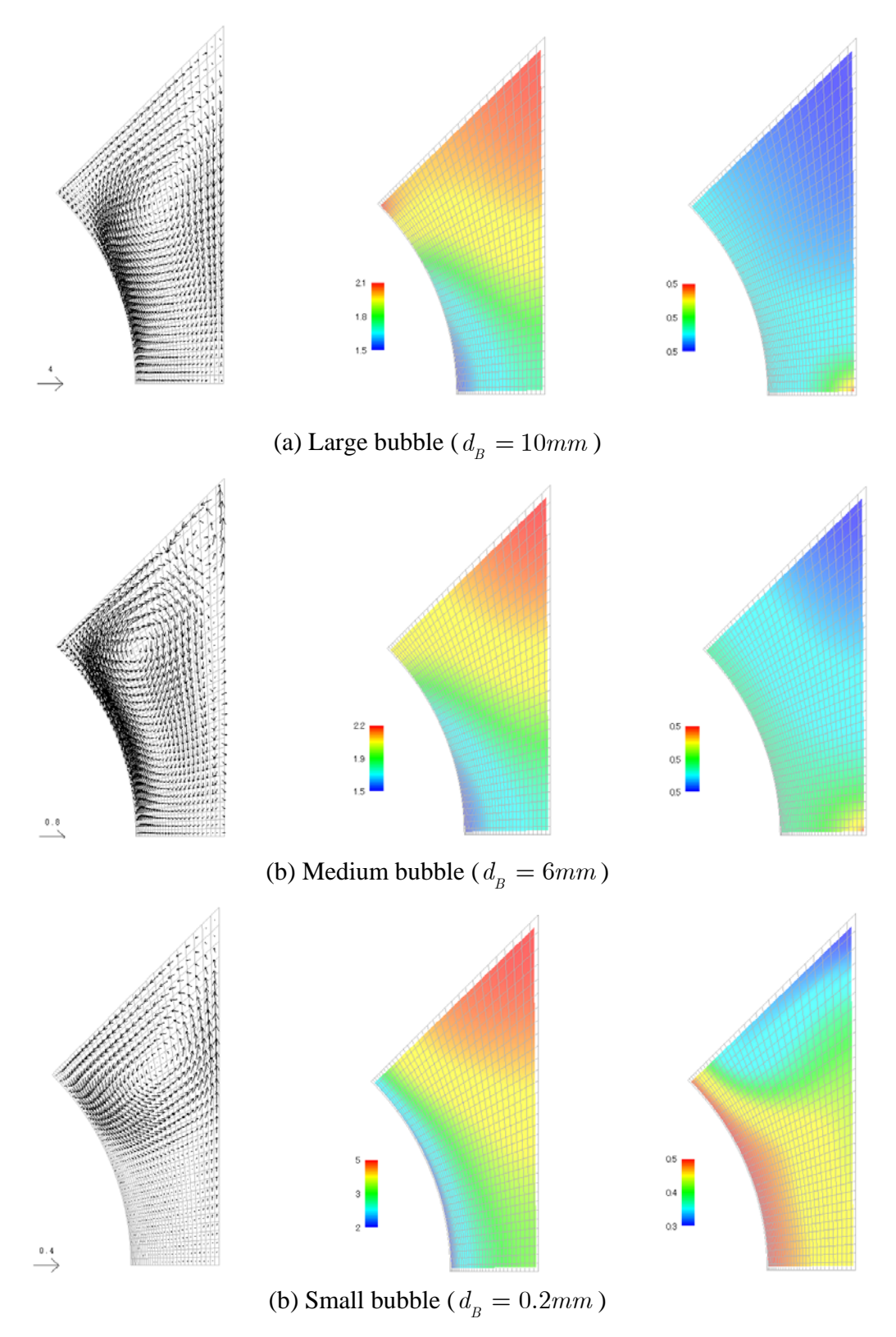


Fig.4 Cross sectional flow (left), axial liquid velocity (middle) and void fraction (right) in subchannel

## 5. Conclusion

Flow structure induced by bubble-liquid interfacial forces was investigated by developing a twodimensional CMFD code. The mass, momentum, turbulence energy and bubble diffusion equations were used as the fundamental equations. Interfacial forces acting in a steady state flow were newly introduced into the momentum equation. Using the generalized coordinate on annular tube and subchannel and an iterative method to keep the symmetry on the nonorthogonal boundary, cross sectional flows induced by the interfacial forces and then void fraction distribution were reasonably calculated.

The void fraction distribution in annular tube and subchannel was compared. Cross sectional flows were not observed in annular tube but in subchannel. In symmetric channels like annular tube, the interfacial forces balanced each other without cross sectional flows; in asymmetric channels like subchannel, they needed another fluid force induced by cross sectional flows. Therefore, the role of the cross sectional flow arose to take the balance between interfacial and fluid forces, and the cross flow was a reason of non-similarity in geometry between channel wall and void fraction distribution.

This study proposed a mechanism for the two-phase fluid interface to break the geometrical similarity of phase distribution in subchannel. Thus the geometrical effect in asymmetric channel is complex. Recent CMFD validation works appear to choose two-phase data taken in symmetric channels like circular or annular tubes. Before its application to asymmetric channels, we should work for explanation of physics, which needs development of multi-dimensional measurement.

#### 6. References

- [1] T. Ikeno and T. Kajishima, Analysis of Dynamical Flow Structure in a Square Arrayed Rod Bundle, Nucl. Eng. Des., in press, doi:10.1016/j.nucengdes.2008.07.012.
- [2] I. Kataoka and A. Serizawa, "Basic equations of Turbulence in Gas-Liquid Two-phase Flow", J. Multiphase Flow, Vol. 15, No.5, pp.843-855 (1989).
- [3] T. Ikeno and I. Kataoka, Numerical simulation of secondary flow in bubbly turbulent flow in sub-channel, Proceedings of the 13th International Topical Meeting on Nuclear Reactor Thermal Hydraulics (NURETH-13),N13P1349, Kanazawa City, Ishikawa Prefecture, Japan, September 27-October 2, (2009).
- [4] Elena A. Tselishcheva, Steven P. Antal, Michael Z. Podowski, Donna Post Guillen, Matthias Beyer, Dirk Lucas, Development and Validation of a Multifield Model of Churn-Turbulent Gas/Liquid Flows, ICONE17-75210, Proceedings of the 17th International Conference on Nuclear Engineering (ICONE-17), July 12-16, Brussels, Belgium (2009).
- [5] I. Kataoka, K.Yoshida, T. Ikeno, T. Sasakawa, K. Kondo, Analysis of Tubulence Structure and Void Fraction Distribution in Gas-liquid Two-phase Flow under Bubbly and Churn Flow Regime, Proceedings of ASME-JSME-KSME Joint Fluids Engineering Conference, AJK2011-10003, July 24-29, Hamamatsu, Shizuoka, JAPAN (2011).

- [6] T. Ikeno, T. Sasakawa, I. Kataoka, Numerical prediction of void distribution in two-phase turbulent flow in a sub-channel, ASME, Journal of Engineering for Gas Turbines and Power, 132, 11, doi:10.1115/1.4001055 (2010)
- [7] S. Kodama and I. Kataoka, "Critical Heat Flux Prediction Method Based on Two-Phase Turbulent Model", *J. Nucl. Sci. Tecnol.*, Vol. 40, No. 10, pp. 725-733 (2003).
- [8] I. Kataoka and A. Serizawa, "Bubble Dispersion Coefficient and Turbulent Diffusivity in Bubbly Two-Phase Flow", Turbulence Modification in Multiphase Flows, *ASME Publication FED*, Vol.110, pp.59-66 (1991).
- [9] M. Ishii, "One Dimensional Drift Flux Model and Constitutive Equations for Relative Motion between Phases in Various Two-Phase Flow Regime", ANL 77-47 (1977).
- [10] I. Kataoka, A. Serizawa and D.C. Besnard, 1993, "Prediction of turbulence suppression and turbulence modeling in bubbly two-phase flow", *Nucl. Eng. Des.*, Vol. 141, pp. 145-158.
- [11] I.Kataoka and A.Serizawa, "Analyses of the Radial Distributions of Average Velocity and Turbulent Velocity of the Liquid Phase in Bubbly Two-Phase Flow", *JSME International Journal*, Series B, 36-3, pp.404-411 (1993).
- [12] I. Kataoka, D.C. Besnard and A. Serizawa, "Basic Equation of Turbulence and Modeling of Interfacial Transfer Terms in Gas-Liquid Two-Phase Flow", *Chemical Engineering Communication*, Vol.118, pp.221-236 (1992).
- [13] L.S. Caretto, A.D. Gosman, S.V. Patankar and D.B. Spalding, "Two calculation procedures for steady three-dimensional flows with recirculation", *Proc. 3rd Int. Conf. on Numerical Methods in Fluid Mech.*, Paris, France, Vol. II. p. 60 (1972).
- [14] N. Kolev, *Multiphase Flow Dynamics 2; Mechanical and Thermal Interactions*, Springer, Tokyo, Japan, pp.483-491 (2002).
- [15] B.J. Yun, B.U.Bae, W.M.Park1, D.J.Euh, G.C.Park, C-.H. Song, Characteristics of local bubble parameters of subcooled boiling flow in an annulus, OECD/NEA & IAEA workshop, Grenoble, France, BOI-02 (2008)